



OPEN

Green synthesis and characterization of α - Mn_2O_3 nanoparticles for antibacterial activity and efficient visible-light photocatalysis

Saeid Taghavi Fardood^{1✉}, Farzaneh Moradnia², Fateme Yekke Zare², Siamak Heidarzadeh³, Mohammad Azad Majedi^{4✉}, Ali Ramazani², Mika Sillanpää^{5,6,7,8,9,10} & Ky Nguyen^{11,12}

In this study, green synthesis, characterizations, photocatalytic performance, and antibacterial applications of α - Mn_2O_3 nanoparticles are reported. The synthesized nanoparticles were characterized by Fourier transform infrared spectroscopy (FT-IR), powder X-ray diffraction (XRD), transmission electron microscope (TEM), Scanning electron microscopy (SEM), energy dispersive X-ray analysis (EDX), Brunauer Emmett Teller (BET), Electrochemical Impedance Spectroscopy (EIS), Photoluminescence (PL), and Differential reflectance spectroscopy (DRS) analysis. The investigation verified that the α - Mn_2O_3 nanoparticles possessed a cubic structure, with a crystallite size of 23 nm. The SEM and TEM techniques were used to study the nanoscale morphology of α - Mn_2O_3 nanoparticles, which were found to be spherical with a size of 30 nm. Moreover, the surface area was obtained as $149.9 \text{ m}^2 \text{ g}^{-1}$ utilizing BET analysis, and the band gap was determined to be 1.98 eV by DRS analysis. The photocatalysis performance of the α - Mn_2O_3 NPs was evaluated for degrading Eriochrome Black T (EBT) dye under visible light and degradation efficiency was 96% in 90 min. The photodegradation mechanism of EBT dye was clarified with the use of radical scavenger agents, and the degradation pathway was confirmed through Liquid Chromatography–Mass Spectrometry (LC–MS) analysis. Additionally, the produced nanoparticles could be extracted from the solution and continued to exhibit photocatalysis even after five repeated runs under the same optimal conditions. Also, the antibacterial activity of green synthesized α - Mn_2O_3 nanoparticles was investigated by using the broth microdilution method towards *Enterococcus faecalis* ATCC 29212 (Gram-positive), *Staphylococcus aureus* ATCC 29213 (Gram-positive), *Salmonella typhimurium* ATCC 14028 (Gram-negative), *Klebsiella pneumoniae* ATCC 7881 (Gram-negative), *Escherichia coli* ATCC 25922 (Gram-negative), *Proteus mirabilis* ATCC 7002 (Gram-negative), and *Pseudomonas aeruginosa* ATCC 27853 (Gram-negative) bacterial strains.

Keywords Green synthesis, Manganese (III) oxide, Photocatalysis, Antibacterial, Eriochrome Black T

¹Department of Chemistry, Faculty of Science, Ilam University, Ilam 69315516, Iran. ²Department of Chemistry, Faculty of Science, University of Zanjan, Zanjan 45371-38791, Iran. ³Department of Microbiology and Virology, School of Medicine, Zanjan University of Medical Sciences, Zanjan, Iran. ⁴Department of Anesthesiology, Faculty of Medicine, Kurdistan University of Medical Sciences, Sanandaj, Iran. ⁵Department of Chemical Engineering, School of Mining, Metallurgy and Chemical Engineering, University of Johannesburg, P. O. Box 17011, Doornfontein 2028, South Africa. ⁶Adnan Kassar School of Business, Lebanese American University, Beirut, Lebanon. ⁷Sustainability Cluster, School of Advanced Engineering, UPES, Bidholi, Dehradun, Uttarakhand 248007, India. ⁸Centre of Research Impact and Outcome, Chitkara University Institute of Engineering and Technology, Chitkara University, Rajpura, Punjab 140401, India. ⁹Department of Civil Engineering, University Centre for Research and Development, Chandigarh University, Gharuan, Mohali, Punjab, India. ¹⁰Division of Research and Development, Lovely Professional University, Phagwara, Punjab 144411, India. ¹¹Institute of Research and Development, Duy Tan University, Da Nang, Vietnam. ¹²School of Engineering and Technology, Duy Tan University, Da Nang, Vietnam. ✉email: s.taghavi@ilam.ac.ir; saeidt64@gmail.com; aa136020062007@yahoo.com

With increasing industrial and agricultural activity, the population growth, global climate change, and diminishing water reserves, environmental concern has been aroused. Synthetic dyes are one of the main water pollutants that have been used in various industries^{1–3}. Researchers have found that these organic dyes have critical threats for environmental and human health because of their persistence and toxicity. So, water treatment is one of the key concerns of the twenty-first century and finding efficient ways is essential^{4–6}. Microbial contamination is another one of the main challenges in food industry and healthcare. Thus, evolution of the antibacterial agents has attracted attention. As reported in the literature, nanoparticles have been used as the useful approach with antibacterial activity^{7–10}.

Photocatalysis is a green, effective, and promising way for the degradation of the organic dyes and other pollutants from wastewaters, because it can convert toxic pollutants into non-toxic compounds under light sources (ultra violet, solar, or visible light)^{11,12}. Photocatalyst attributes such as band gap, light-harvesting performance, surface area, and morphology have main roles in photocatalytic performance^{13–15}. Therefore, developing and synthesizing photocatalyst with high performance is essential for degrading organic dyes in wastewater^{16,17}.

Different methods, such as sol–gel, hydrothermal, sonochemical, microemulsion, co-precipitation, biological synthesis, have been used for nanoparticles synthesis^{18–21}. Synthesis of nanoparticles by using plant extracts has attracted attention since it is environmentally friendly, non-toxic, inexpensive, simple, and efficient method^{22–26}. In 2020, Chandiran et al. reported the synthesis of α - Mn_2O_3 nanorods via the hydrothermal route. They then investigated the effectiveness of these nanorods for the decolorization of methylene blue and rhodamine B dyes as cationic dyes²⁷. Gnanam group reported the preparation of alpha manganese sesquioxide (α - Mn_2O_3) by hydrothermal method and investigated them for the photodegradation of ye Remazol Red B dye using a multilamp photo reactor²⁸.

In this work, α - Mn_2O_3 NPs were prepared with the green sol–gel method by using tragacanth gel (TG), as the natural gel. The synthesized nanoparticles were characterized by FTIR, XRD, DRS, BET, TEM, FESEM, EIS, PL, and EDX analysis. The photocatalytic activity of α - Mn_2O_3 NPs was considered for the degradation of Eriochrome Black T (EBT) dye under the visible light irradiation. Moreover, Radical scavenger agents and LC–MS analysis validated EBT dye's photodegradation mechanism. Different Gram-positive bacterial strains such as *Enterococcus faecalis* ATCC 29212, *Staphylococcus aureus* ATCC 29213, and Gram-negative bacterial strains consist of *Escherichia coli* ATCC 25922, *Salmonella typhimurium* ATCC 14028, *Klebsiella pneumoniae* ATCC 7881, *Proteus mirabilis* ATCC 7002, and *Pseudomonas aeruginosa* ATCC 27853 were selected as bacterial models to evaluation the antimicrobial activity of synthesized α - Mn_2O_3 nanoparticles. The molecular structure of the EBT dye is shown in Fig. 1.

Experimental

Materials and characterization

The tragacanth gum (TG), Eriochrome Black T dye, $Mn(NO_3)_2 \cdot 4H_2O$ with Purity: $\geq 99\%$, and bacterial strains were purchased from health food shop, Alvansabet Company (Iran), and Dae-Jung (Korea), Merck (Germany), respectively. The XRD pattern was collected on an X'Pert-PRO advanced diffractometer with Cu-K α radiation (wavelength: 1.5406 Å) of 40 kV and 40 mA by step scanning in an angle range of $10^\circ \leq 2\theta \leq 80^\circ$ at ambient temperature. Using a Metrohm (Analytik Jena-Specord 205) double-beam instrument, UV–Vis absorption spectra were obtained. The Jasco 6300 spectrophotometer recorded the α - Mn_2O_3 NPs' FTIR spectra at a resolution of 4 cm^{-1} . BET analysis was achieved with the Belsorp Mini II to determine the specific surface area of prepared sample. optical properties were recorded by UV–vis diffuse reflectance spectra (Shimadzu, UV-2550, Japan), and band gap (E_g) was calculated by the Tauc's theory²⁹. TEM was recorded with EM 208S, and SEM coupled by energy dispersive X-ray EDX was investigated with Tescan Mira3. Electrochemical impedance spectroscopy (EIS) was recorded by μ -AUTOLAB electrochemical system type III (Eco-Chemio, Switzerland). The ensuing degradation products of EBT dye were analyzed using a Waters Alliance 2695 HPLC–Micromass Quattro micro API Mass Spectrometer. A Cary Eclipse Fluorescence Spectrometer with a Xe lamp excitation source was used to record room-temperature photoluminescence (PL) spectra.

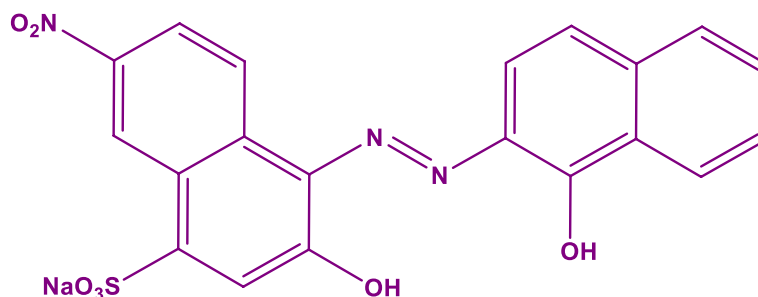


Figure 1. Molecular structure of Eriochrome Black T dye.

Synthesis the α -Mn₂O₃ nanoparticles

Firstly, TG solution was prepared based on our previous work³⁰. Then 1.5 g of Mn(NO₃)₂·4H₂O were added into the TG solution and the container was moved to the sand bath set at 75 °C, for 12 h under stirring. The dried resin was calcined at 500 °C for 4 h to obtain α -Mn₂O₃ nanoparticles.

Photocatalytic experiment

The photocatalytic performance of α -Mn₂O₃ nanoparticles were investigated under visible light with fluorescent lamp ($\lambda > 400$, 90 W, Parmis, Iran). The photocatalytic experiments for the degradation of the EBT dye were monitored in 50 ml solution and the effects of visible light irradiation, dark, initial dye concentration (20–50 mg L⁻¹) photocatalyst dosage (0.02–0.05 g), time (0–90 min), and pH (3, natural, and 9) were studied to find the best degradation efficiency. The degradation efficiency of EBT dye was calculated by UV–Vis spectrophotometer at the $\lambda_{\max} = 546$ nm.

Antimicrobial experiment

Minimum inhibitory concentration

The minimum inhibitory concentrations (MICs) of α -Mn₂O₃ nanoparticle synthesized was evaluated by broth microdilution method against Gram-positive and Gram-negative bacteria. Bacterial strains were separately cultured at 37 °C for 24 h in 5 ml Brain heart infusion (BHI) broth (Merck, Germany). Then, the bacteria were diluted to the 0.5 McFarland standard (1.5×10^8 CFU/ml). Mueller–Hinton broth (200 μ l) was added to all 96 microplate wells. The stock concentrations of α -Mn₂O₃ nanoparticle were serially diluted to obtain concentrations in the range of 1–5 μ g/ml. Approximately 100 μ l of α -Mn₂O₃ nanoparticle (1–5 μ g/ml) was then serially diluted in 1% dimethyl sulfoxide (DMSO) in the 96 wells microplate row-to-row. After that, the prepared bacterial suspension (100 μ l) of 0.5 McFarland standard was added to all of the microplate wells and then incubated for 18 h at 37 °C in a shaker incubator at 120 rpm. The MIC was determined as the lowest concentration that inhibited visible bacterial growth observed within the microplate.

The minimum bactericidal concentration

The MBC is the minimum concentration of the nanoparticle that is bactericidal. MBC is determined as the lowest broth dilution of α -Mn₂O₃ nanoparticle that inhibits growth of the bacteria on the agar plate. The lack of bacterial growth in the Müller–Hinton agar was indicative of MBC.

MBC was measured by sub-culturing the broth dilutions applied for MIC determination on agar media. Briefly, 50 μ l of broth dilutions of MIC was sub-culturing onto Müller–Hinton agar (Merck, Germany) and incubated overnight at 37 °C. The lowest broth dilution of nanoparticles that inhibits the growth of bacteria on the agar plate is known as MBC. The lack of bacterial growth in the Mueller–Hinton agar was indicative of MBC.

Result and discussion

Characterization

Figure 2a demonstrates the XRD pattern of the α -Mn₂O₃ nanoparticles. It is evident that sharp and strong diffraction peaks are assigned to cubic structure of synthesized sample (JCPDS card no. 89-4836). Based on the XRD pattern, the crystalline size of α -Mn₂O₃ NPs was appraised by Scherrer equation^{31,32} and the obtained value is 23 nm. XRD pattern without characteristic peaks of impurities, confirms the effective synthesis of the α -Mn₂O₃ NPs by this green method.

The FTIR spectrum of the synthesized α -Mn₂O₃ NPs is given in Fig. 2b. The bands at 3420 and 1624 cm⁻¹ corresponds to the O–H stretching and H₂O bending vibration of the free and absorbed water molecule²⁹. Also, the absorption peaks located at 517, 572, 664 cm⁻¹ are specified to the vibrational bond of Mn–O, that corroborates successful synthesis of α -Mn₂O₃ nanoparticles^{28,33}. The nitrogen adsorption–desorption isotherm of α -Mn₂O₃ NPs is given in Fig. 2c, and approved the typical type IV with hysteresis loops type H1 based on the IUPAC classification³⁴. Moreover, the BET surface area, pore volume, and pore size of sample were found to be 149.9 m² g⁻¹, 7.02 nm, and 0.2525 cm³ g⁻¹, respectively. Also, The BJH curve, which is exposed in Fig. 2d, shows that the pores in α -Mn₂O₃ NPs have an average size of 2 nm.

The TEM and FESEM analysis were carried out to investigate the morphology and size of synthesized nanoparticles and their results are shown in Fig. 3. It is clear that α -Mn₂O₃ NPs have a uniform distribution and spherical shape with the average size of 30 nm. Moreover, the EDX pattern confirmed the existence of Manganese (Mn), and oxygen (O) elements in as-prepared sample (Fig. 4).

The UV–Vis–DRS spectrum and tauc plot of the synthesized α -Mn₂O₃ NPs are shown in Fig. 5a. Based on the result, the bandgap of sample is about 1.98 eV. This narrow bandgap confirms that synthesized nanoparticles can be suitable for photocatalysis under the visible light irradiation.

EIS was conducted with a 5 mV AC amplitude in the frequency range of 100 kHz–0.1 Hz under open circuit potential. Figure 5b displays Nyquist plots and comparable circuits for bare carbon fabric (a) and α -Mn₂O₃/carbon cloth (b). The intersection of the curves at the real portion Z' (Re) represents a combination of intrinsic resistance of the electrode material, ionic resistance of the electrolyte, and contact resistance at the active material/carbon fabric interface. The Re value for α -Mn₂O₃/carbon cloth (7.8 Ω) is comparable to that of bare carbon cloth (6.9 Ω), indicating low intrinsic resistance of the electrode material. Furthermore, α -Mn₂O₃/carbon cloth exhibits a low charge-transfer resistance (Rct) of 1.09 Ω , suggesting facile charge-transfer kinetics for the produced α -Mn₂O₃ NPs.

Figure 5c shows the room temperature PL spectra of α -Mn₂O₃ NPs under laser excitation at 280 nm. The emission at 561 nm is the result of a single ionized oxygen vacancy, which leads to the green emission of the sample due to the recombination of a hole with a single ionized electron in the valence band. This oxygen vacancy

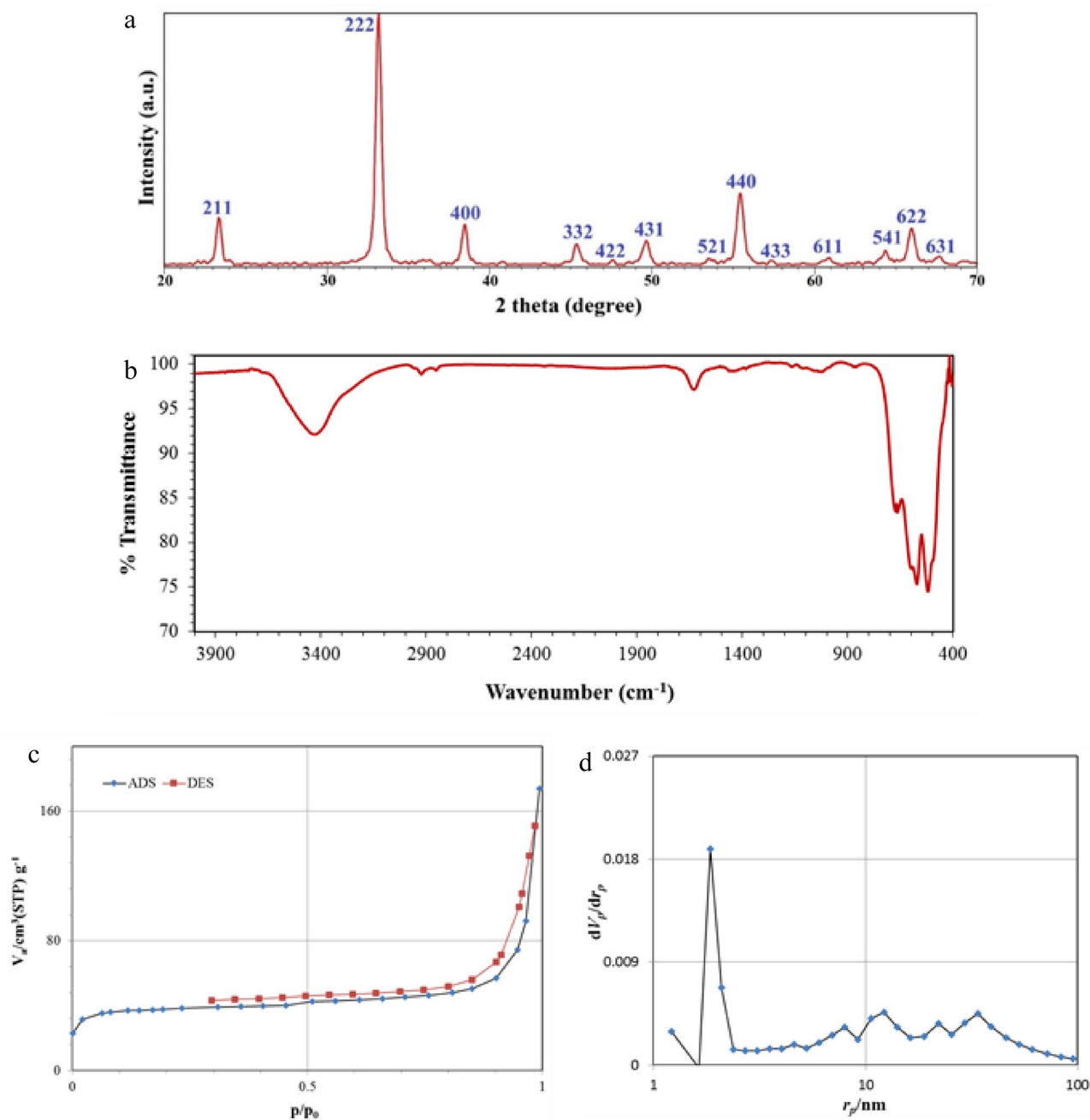


Figure 2. (a) XRD pattern, (b) FT-IR spectrum, (c) The N_2 absorption/desorption isotherm, (d) BJH curve of the α - Mn_2O_3 NPs.

is closely associated with the photocatalytic activity of α - Mn_2O_3 in degrading EBT. Moreover, numerous studies in the literature have highlighted the role of oxygen vacancies in enhancing photocatalytic reactions^{35,36}.

Photocatalytic activities

To investigate the photocatalytic activity of synthesized sample, α - Mn_2O_3 NPs was used in photodegradation experiments toward EBT dyes and obtained results are given in detail.

Photocatalyst dosage is one of the important factors in the performance of dye degradation³⁷. So, the effect of photocatalyst amount was studied in the range of 0.02–0.05 g of α - Mn_2O_3 NPs, at a constant concentration of EBT (40 mg L^{-1}) and irradiation time (90 min). As specified in Fig. 6a, the degradation efficiency of EBT raises from 69 to 97% with increasing photocatalysis dosage up from 0.02 to 0.05 g. This may be due to enhance of active sites on the surface of nanoparticles, penetration of visible light radiation into the suspension, and free electrons generation in the conduction band^{38,39}. So, next experiments were conducted by using 0.04 g of sample as the best dosage.

To find the effect of initial dye concentration, degradation efficiency was investigated in different concentration of EBT dye (20–50 mg L^{-1}). As shown in Fig. 6b, rate of degradation decreased from 96 to 88% in 90 min,

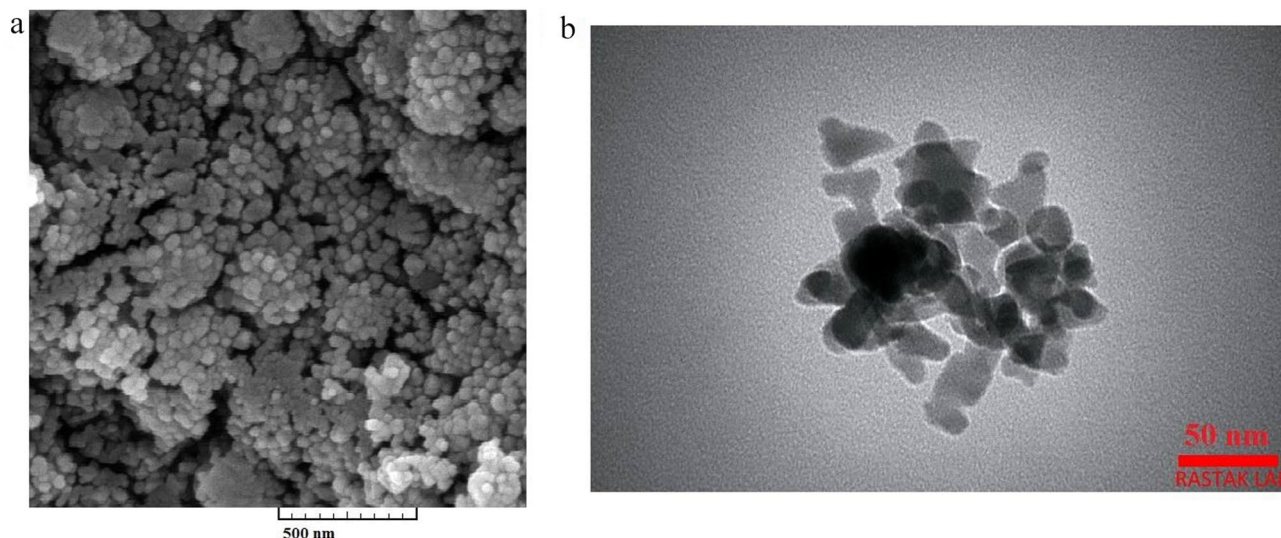


Figure 3. (a) FESEM image and (b) TEM image of α - Mn_2O_3 NPs.

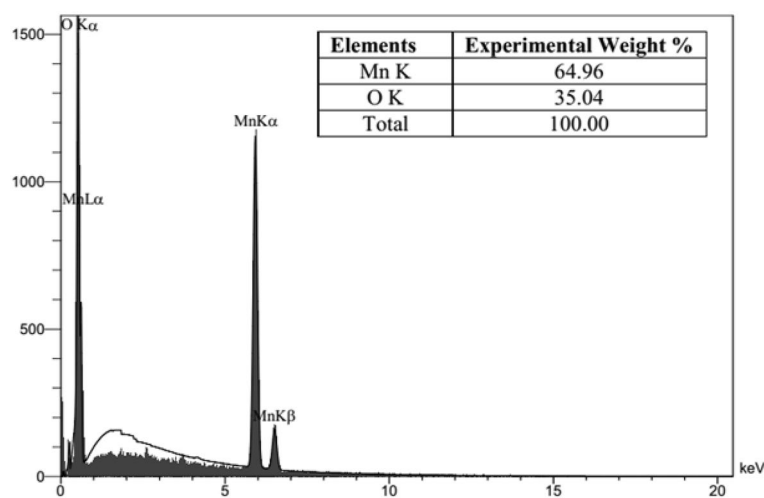


Figure 4. EDX pattern of α - Mn_2O_3 NPs.

when the initial concentration of dye increased from 40 to 50 mg L⁻¹. At high concentration, dye molecules inhibit as the penetration and absorption of photons on the surface of the catalyst; for this reason, the degradation rate decreased^{37,40}. Thus, the following experiments were conducted by 40 mg L⁻¹ of EBT concentration as the best concentration.

To obtain the best irradiation time, the photodegradation study was monitored at diverse time gaps, and obtained result is given in Fig. 6c. The lambda max of EBT dye is placed at 546 nm. Degradation performance was verified with decline in absorbance maximum values while irradiation time increased. It is evident that 96% of EBT dye was removed in 90 min.

Photocatalytic activity of α - Mn_2O_3 NPs for dye degradation was proved with checking the efficiency in three states; photolysis (visible light irradiation without α - Mn_2O_3 NPs), adsorption (α - Mn_2O_3 NPs under dark), and photocatalysis (α - Mn_2O_3 NPs under visible light irradiation). In photolysis state, dye degradation was not observed. In adsorption condition, we have dye removal of 54%. As shown in Fig. 6d, in photocatalysis state 96% of EBT dye was removed at 90 min. These results corroborate the high photocatalytic activity of synthesized nanoparticles for EBT degradation under visible light in ambient condition. Figure 6e provides the photodegradation of EBT dye in the presence of α - Mn_2O_3 at various pH levels and times. Based on the chart, the highest level of degradation occurs at alkaline pH. However, significant degradation is also observed at neutral pH, indicating the high activity of the photocatalyst. At higher pH values, the concentration of hydroxyl ions increases, resulting in a greater presence of hydroxyl radicals in the medium and consequently faster degradation.

To investigate the photodegradation mechanism of EBT dye in the presence of α - Mn_2O_3 as the photocatalyst and identify the main reactive species involved, radical trapping studies were conducted (Fig. 6f). The diagram demonstrates that the presence of p-benzoquinone (p-BQ), NaN₃, and KI resulted in a reduction of

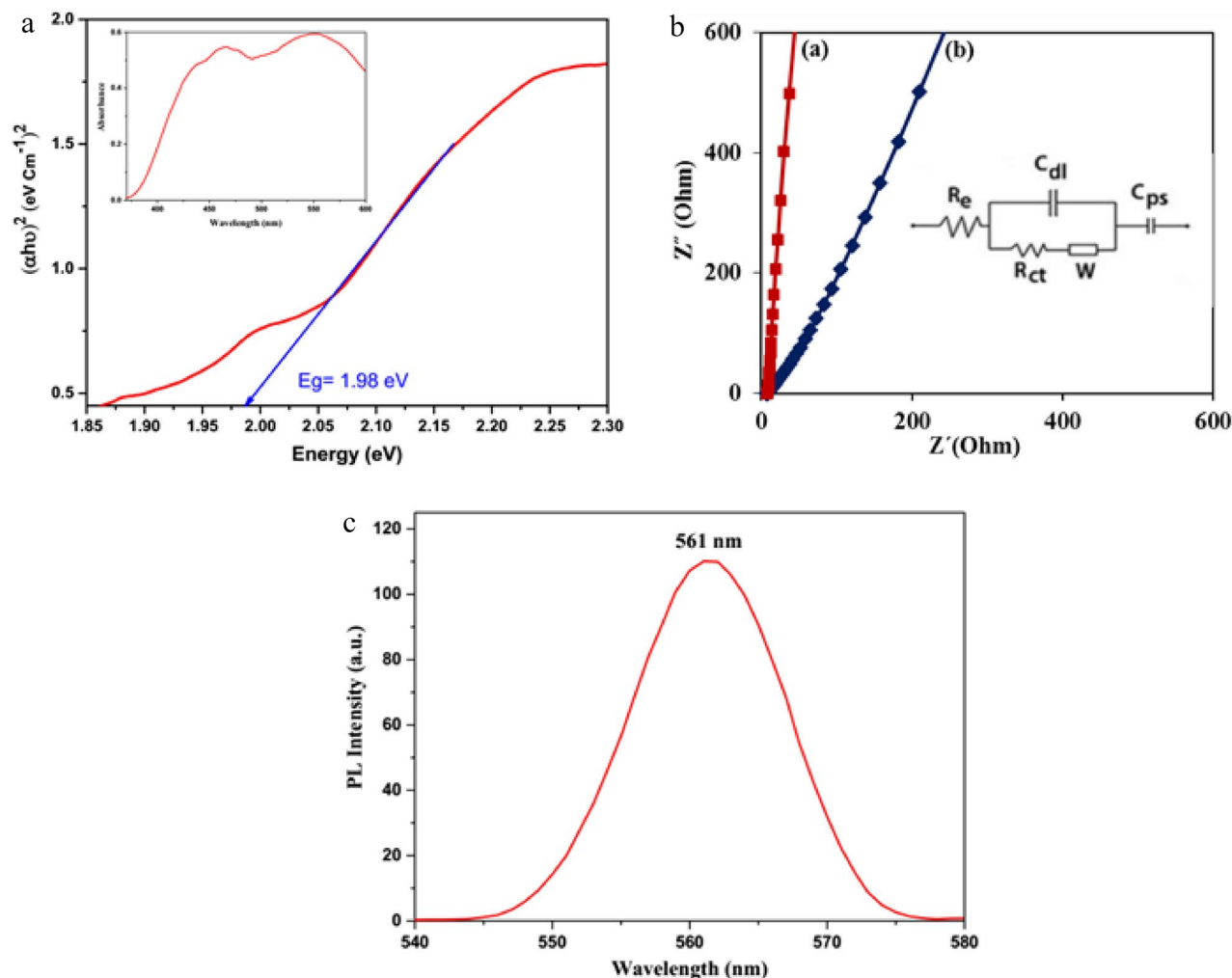


Figure 5. (a) UV-Vis-DRS (inset) and Tauc plot, (b) the EIS curves of carbon cloth (a) and α -Mn₂O₃/carbon cloth (b) in 1 M KOH and related the equivalent circuit model (inset), (c) PL spectra of α -Mn₂O₃ NPs.

the degradation efficiency (DE%) from 96 to 92%, 37%, and 68% respectively, after a duration of 90 min. These substances act as radical scavengers for the superoxide radical, singlet oxygen, and hydroxyl radical respectively. It is evident that singlet oxygen has a more significant role in the breakdown mechanism of EBT dye compared to superoxide radical and hydroxyl radical. Figure 7 illustrates the proposed process for the breakdown of EBT dye using LC-Mass analysis. The findings show that there was a breakdown of the EBT dye molecules, leading to the creation of smaller fragmented molecules. Table 1 reports on these broken molecules.

The photodegradation of pollutants often follows first-order reaction kinetics, described by the relationship between the degradation rate and the irradiation time (t) as $\ln(C_0/C_t) = kt$, where k is the reaction rate constant⁴¹. Figure 8a illustrates the kinetics of EBT dye photodegradation by α -Mn₂O₃ nanoparticles. The rate constant for EBT dye degradation is $k = 0.0254 \text{ min}^{-1}$, as determined from the slope of the line. Photocatalytic degradation of EBT dye solution can be accomplished by repeated use of the α -Mn₂O₃ catalyst. The photocatalytic degradation of EBT under visible light irradiation was measured to assess the reusability of this catalyst. Following centrifugation, washing with distilled water under ultrasonic irradiation, and reusing the photocatalyst for consecutive runs. The photocatalytic efficiency of α -Mn₂O₃ nanoparticles experiences a modest decline after undergoing five cycles of use. In Fig. 8b, the photodegradation rates for recycling runs 1–5 were 96%, 96%, 95%, 93%, and 93% respectively. The stability of α -Mn₂O₃ NPs was found during the process of photocatalytic oxidation.

The photodegradation capabilities of synthesized α -Mn₂O₃ NPs were compared to other photocatalysts for EBT dye degradation to illustrate their efficiency and relevance. Table 2 compares the efficiency of α -Mn₂O₃ NPs to different photocatalysts. This work goes beyond method innovation and photocatalytic efficiency to offer significant advantages above earlier publications. Water and tragacanth gum are used to synthesize nanoparticles in an eco-friendly, cost-effective, and simple process. The produced α -Mn₂O₃ NPs demonstrate stability, recyclability, and EBT degradation efficiency.

Antibacterial activity

The amount of bacteria inhibited by α -Mn₂O₃ were variable, among which *S. aureus* and *E. faecalis* (1 $\mu\text{g/mL}$) were significantly inhibited, and *E. coli*, *K. pneumoniae*, and *P. mirabilis* (2.5 $\mu\text{g/mL}$) were moderately inhibited.

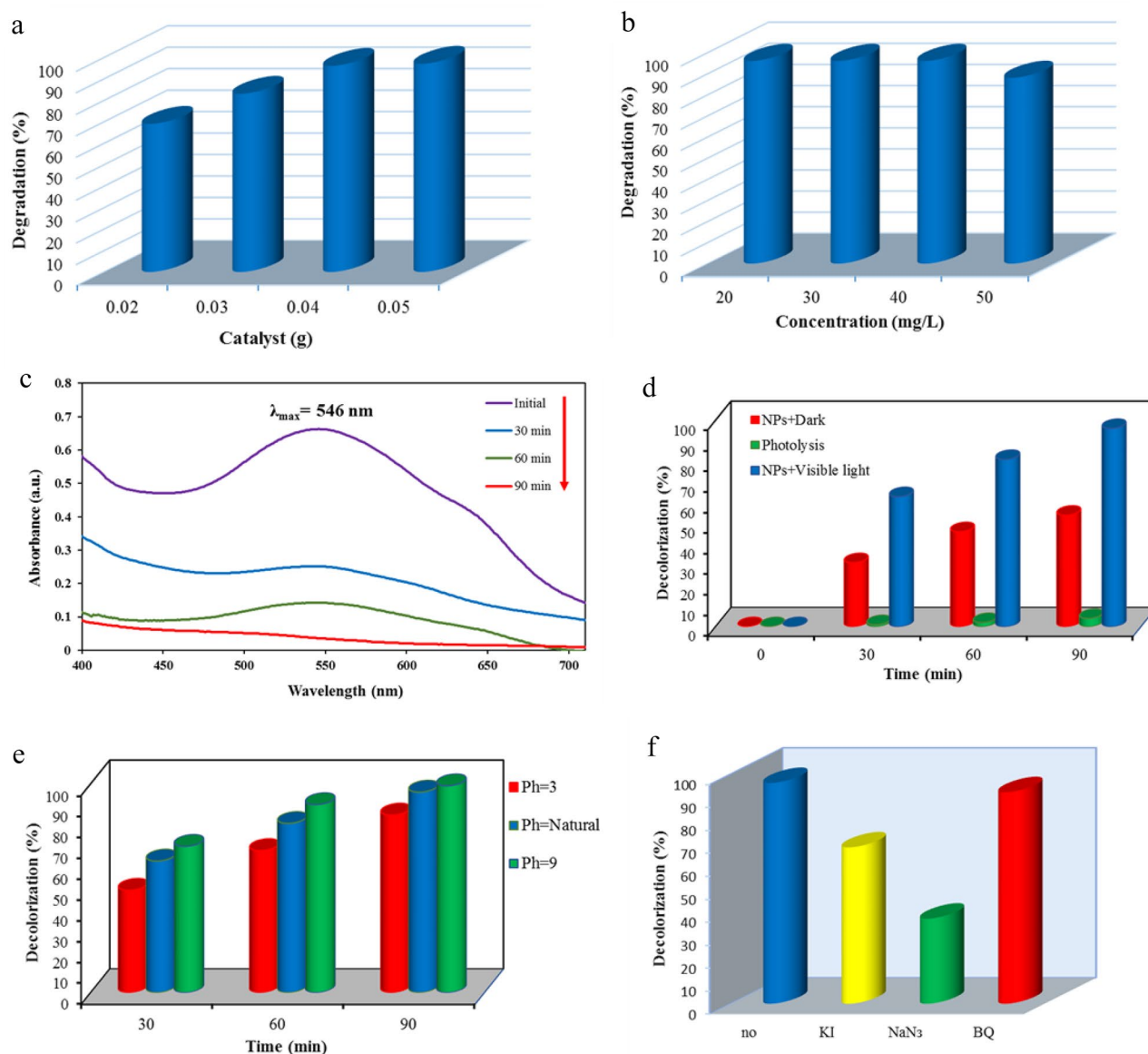


Figure 6. (a) The impact of photocatalyst dosage on EBT degradation, pH = natural, EBT = 40 mg/L, (b) impact of initial concentration on the degradation efficiency (%), pH = natural, amount of catalyst = 0.04 g, (c) Absorption spectra of EBT solutions under visible light radiation, pH = natural, EBT = 40 mg/L, catalyst = 0.04 g. (d) Impact of visible light irradiation, pH = natural, EBT = 40 mg/L, catalyst = 0.04 g, 90 min, (e) impact of pH on the degradation efficiency. (f) Assessing EBT degradation efficiency in various radical scavenger.

However, *P. aeruginosa* and *S. typhimurium* (3.5 $\mu\text{g}/\text{mL}$) were weakly inhibited by $\alpha\text{-Mn}_2\text{O}_3$. The highest MBC of $\alpha\text{-Mn}_2\text{O}_3$ was observed against *S. aureus* and *E. faecalis* (2 $\mu\text{g}/\text{mL}$). The MBC of $\alpha\text{-Mn}_2\text{O}_3$ against *E. coli* and *P. mirabilis* was 3 $\mu\text{g}/\text{mL}$, and against *K. pneumonia* was 3.5 $\mu\text{g}/\text{mL}$. However, MBC was not detected against *P. aeruginosa* and *S. typhimurium* (Table 3).

Based on the results, the synthesized nanoparticles exhibited more inhibitory and lethal properties against gram-positive bacteria than gram-negative bacteria, possibly owing to the cellular envelope structure in gram-negative bacteria, because these bacteria have additional outer membrane and porin or porin-like proteins in their envelope structure. The presence of these structures in gram-negative bacteria gives them the ability to selectively enter hydrophobic and hydrophilic molecules inside the bacteria and thus protects the bacterial cell from antibacterial substances.

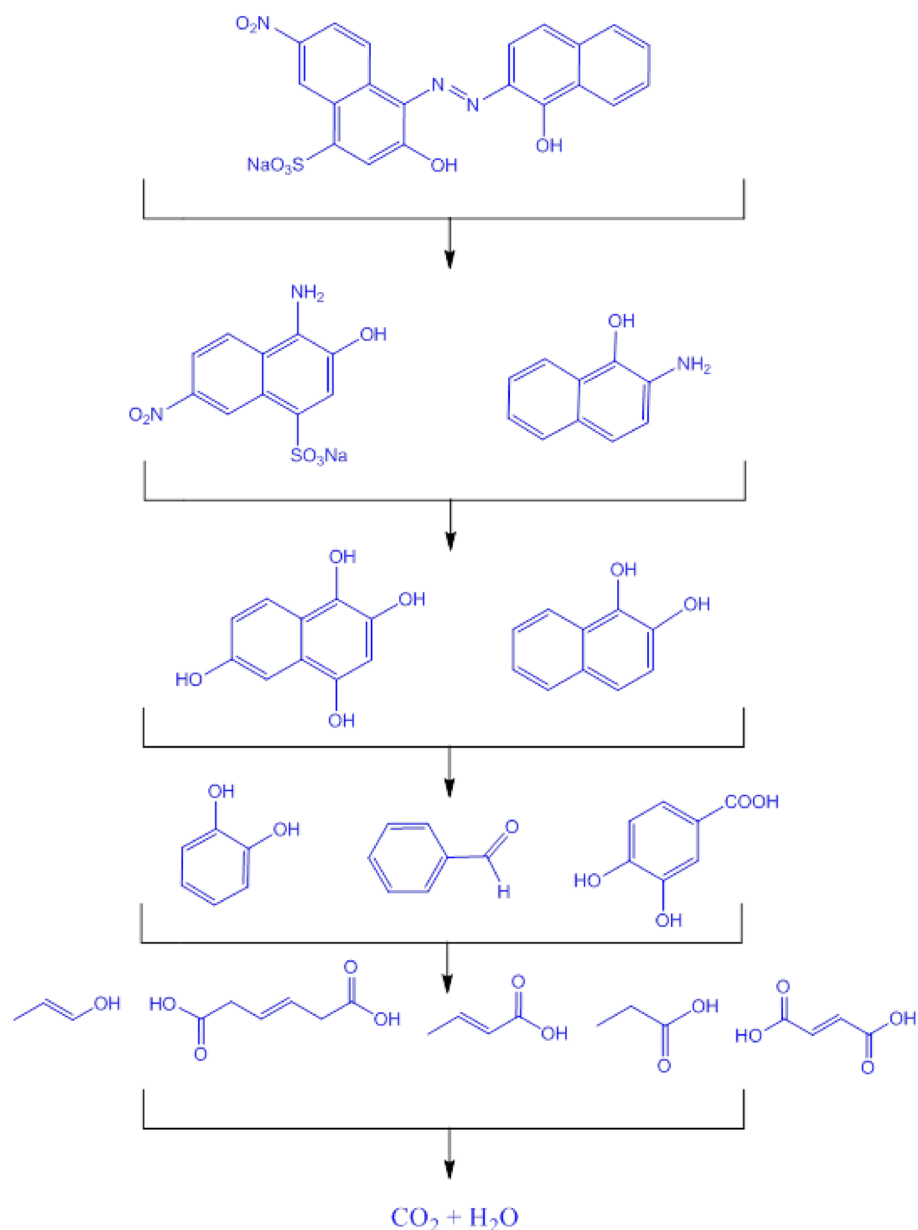


Figure 7. Proposed pathway for EBT degradation using $\alpha\text{-Mn}_2\text{O}_3$.

Conclusions

The $\alpha\text{-Mn}_2\text{O}_3$ nanoparticle was successfully prepared by the green and facile sol–gel method without using surfactants and organic solvents. The successful synthesis of the nanoparticles was confirmed by FTIR, XRD, BET, DRS, PL, EIS, TEM, FESEM, and EDX techniques. Based on the XRD and BET analysis, $\alpha\text{-Mn}_2\text{O}_3$ NPs were prepared in pure cubic structure and high surface area ($149.9\text{ m}^2\text{ g}^{-1}$). Also, SEM and TEM images revealed that morphology of nanoparticles is spherical with average width of 30 nm. The photocatalytic activity was verified by comparing the photocatalysis activity with adsorption and photolysis, suggesting a synergistic effect between prepared nanoparticles and visible light toward EBT dye degradation. An analysis of the degradation products of the EBT dye was conducted using LC–MS and proposed pathway for EBT degradation was suggested. The $\alpha\text{-Mn}_2\text{O}_3$ nanoparticles had appropriate antibacterial activity and showed greater inhibitory and lethal properties against gram-positive bacteria than gram-negative bacteria. This simple method, using renewable tree gum materials and abundant natural resources to prepare the reusable catalyst, would inspire further research into producing and recycling friendly catalysts to degrade different pollutants using abundant light.


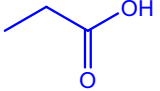
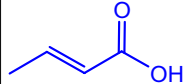
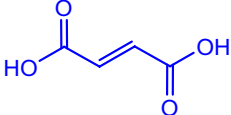
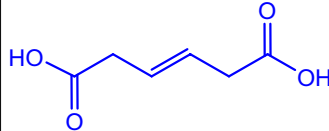
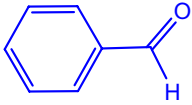
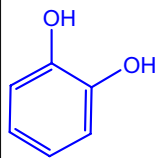
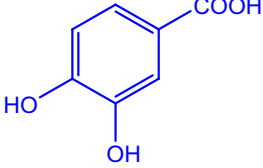
No	Structure	m/z	No	Structure	m/z
1		58	2		74
3		86	4		115
5		143	6		105
7		110	8		154

Table 1. Identification of by-Products formed during the photocatalytic degradation of EBT.

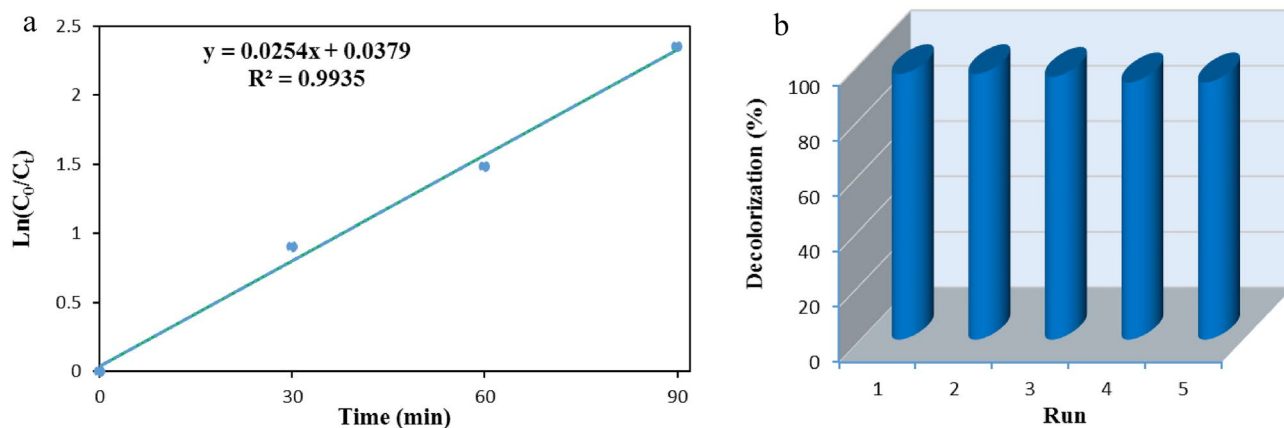


Figure 8. (a) Pseudo-first-order kinetic plot for the decolorization of EBT. (b) Reusability of α - Mn_2O_3 photocatalyst for the decolorization of EBT.

Catalysts	Dye concentration (mg/L)	Light source	Irradiation time (min)	Degradation efficiency (%)	Refs
$CoCr_2O_4$	20	Visible light	90	90	37
TiO_2 (PC-50)	25	UV-light	90	35	42
TiO_2 (PC-500)	25	UV-light	90	51	42
ZnO (Merck)	25	UV-light	90	62	42
TiO_2	25	UV-light	90	82	42
SnO_2 -bentonite	100	UV-light	300	100	43
$ZnO@Ag_2S$	40	UV-light	120	69	44
$TiO_2@CNTs$	100	UV-light	100	92	45
$TiO_2@CNTs$	100	Visible light	100	88	45
α - Mn_2O_3	40	Visible light	90	96	This study

Table 2. Photodegradation comparison of EBT with diverse photocatalysts.

Organism	ATCC	Types of bacteria	MIC of α -Mn ₂ O ₃ (μ g/mL)	MBC of α -Mn ₂ O ₃ (μ g/mL)	Control (1% DMSO)
<i>Staphylococcus aureus</i>	29213	Gram-positive	1	2	Not active
<i>Enterococcus faecalis</i>	29212	Gram-positive	1	2	Not active
<i>Escherichia coli</i>	25922	Gram-negative	2.5	3	Not active
<i>Salmonella typhimurium</i>	14028	Gram-negative	3	Not determined	Not active
<i>Klebsiella pneumoniae</i>	7881	Gram-negative	2.5	3.5	Not active
<i>Proteus mirabilis</i>	7002	Gram-negative	2.5	3	Not active
<i>Pseudomonas aeruginosa</i>	27853	Gram-negative	3	Not determined	Not active

Table 3. MIC and MBC of α -Mn₂O₃ nanoparticle against range of pathogenic bacteria.

Data availability

The datasets used and/or analyzed during the current study are available from the corresponding author on reasonable request.

Received: 27 October 2023; Accepted: 8 March 2024

Published online: 21 March 2024

References

- Roy, H. *et al.* Toxic dye removal, remediation, and mechanism with doped SnO₂-based nanocomposite photocatalysts: A critical review. *J. Water Process. Eng.* **54**, 104069 (2023).
- Kaur, P. *et al.* Photoelectrocatalytic treatment of municipal wastewater with emerging concern pollutants using modified multi-layer catalytic anode. *Chemosphere* **339**, 139575 (2023).
- Moradi, M., Vasseghian, Y., Arabzade, H. & Khaneghah, A. M. Various wastewaters treatment by sono-electrocoagulation process: A comprehensive review of operational parameters and future outlook. *Chemosphere* **263**, 128314 (2021).
- Khataee, A. *et al.* Cu₂O-CuO@biochar composite: Synthesis, characterization and its efficient photocatalytic performance. *Appl. Surf. Sci.* **498**, 143846. <https://doi.org/10.1016/j.apsusc.2019.143846> (2019).
- Selvaraj, V., Karthika, T. S., Mansiya, C. & Alagar, M. An over review on recently developed techniques, mechanisms and intermediate involved in the advanced azo dye degradation for industrial applications. *J. Mol. Struct.* **1224**, 129195 (2021).
- Ajmal, A., Majeed, I., Malik, R. N., Idriss, H. & Nadeem, M. A. Principles and mechanisms of photocatalytic dye degradation on TiO₂ based photocatalysts: A comparative overview. *RSC Adv.* **4**, 37003–37026 (2014).
- Sirelkhatim, A. *et al.* Review on zinc oxide nanoparticles: Antibacterial activity and toxicity mechanism. *Nano-Micro Lett.* **7**, 219. <https://doi.org/10.1007/s40820-015-0040-x> (2015).
- Tripathi, N. & Goshisht, M. K. Recent advances and mechanistic insights into antibacterial activity, antibiofilm activity, and cytotoxicity of silver nanoparticles. *ACS Appl. Bio Mater.* **5**, 1391–1463 (2022).
- Das, C. A. *et al.* Antibacterial activity of silver nanoparticles (biosynthesis): A short review on recent advances. *Biocatal. Agric. Biotechnol.* **27**, 101593 (2020).
- Taghavi Fardood, S., Moradnia, F. & Ramazani, A. Green synthesis and characterisation of ZnMn₂O₄ nanoparticles for photocatalytic degradation of Congo red dye and kinetic study. *Micro Nano Lett.* **14**, 986–991 (2019).
- Hao, M., Meng, X. & Miao, Y. Synthesis of NiWO₄ powder crystals of polyhedron for photocatalytic degradation of Rhodamine. *Solid State Sci.* **72**, 103. <https://doi.org/10.1016/j.solidstatesciences.2017.08.018> (2017).
- Ruziwa, D. T. *et al.* Pharmaceuticals in wastewater and their photocatalytic degradation using nano-enabled photocatalysts. *J. Water Process Eng.* **54**, 103880 (2023).
- Vijayan, K. & Vijayachamundeswari, S. Improving the multifunctional attributes and photocatalytic dye degradation of MB and RhB dye—A comparative scrutiny. *Inorg. Chem. Commun.* **144**, 109940 (2022).
- Liqiang, J. *et al.* Review of photoluminescence performance of nano-sized semiconductor materials and its relationships with photocatalytic activity. *Sol. Energy Mater. Sol. Cells* **90**, 1773–1787 (2006).
- Zinatloo-Ajabshir, S., Baladi, M., Amiri, O. & Salavati-Niasari, M. Sonochemical synthesis and characterization of silver tungstate nanostructures as visible-light-driven photocatalyst for waste-water treatment. *Sep. Purif. Technol.* **248**, 117062 (2020).
- Liu, F., Leung, Y. H., Djuricic, A. B., Ng, A. M. C. & Chan, W. K. Native defects in ZnO: Effect on dye adsorption and photocatalytic degradation. *J. Phys. Chem. C* **117**, 12218–12228 (2013).
- Jasrotia, R. *et al.* Photocatalytic dye degradation efficiency and reusability of Cu-substituted Zn-Mg spinel nanoferrites for wastewater remediation. *J. Water Process Eng.* **48**, 102865 (2022).
- Raeisi Shahraki, R. & Ebrahimi, M. Synthesize of superparamagnetic zinc ferrite nanoparticles at room temperature. *J. Nanostruct.* **2**, 413–416 (2012).
- Beshkar, F. & Salavati-Niasari, M. Facile synthesis of nickel chromite nanostructures by hydrothermal route for photocatalytic degradation of acid black 1 under visible light. *J. Nanostruct.* **5**, 17–23 (2015).
- Moradnia, F., Taghavi Fardood, S., Ramazani, A., Osali, S. & Abdolmaleki, I. Green sol-gel synthesis of CoMnCrO₄ spinel nanoparticles and their photocatalytic application. *Micro Nano Lett.* **15**, 674–677. <https://doi.org/10.1049/mnl.2020.0189> (2020).
- Król, A., Pomastowski, P., Rafińska, K., Railean-Plugaru, V. & Buszewski, B. Zinc oxide nanoparticles: Synthesis, antiseptic activity and toxicity mechanism. *Adv. Colloid Interface Sci.* **249**, 37–52 (2017).
- Aljabali, A. *et al.* Synthesis of gold nanoparticles using leaf extract of *Ziziphys zizyphus* and their antimicrobial activity. *Nanomaterials* **8**, 174 (2018).
- Taghavi Fardood, S., Moradnia, F., Heidarzadeh, S. & Naghipour, A. Green synthesis, characterization, photocatalytic and antibacterial activities of copper oxide nanoparticles of copper oxide nanoparticles. *Nanochem. Res.* **8**, 134 (2023).
- Nieto-Maldonado, A. *et al.* Green synthesis of copper nanoparticles using different plant extracts and their antibacterial activity. *J. Environ. Chem. Eng.* **10**, 107130 (2022).
- Moradnia, F., Taghavi Fardood, S. & Ramazani, A. Green synthesis and characterization of NiFe₂O₄@ZnMn₂O₄ magnetic nanocomposites: An efficient and reusable spinel nanocatalyst for the synthesis of tetrahydropyrimidine and polyhydroquinoline derivatives under microwave irradiation. *Appl. Organomet. Chem.* **38**, e7315. <https://doi.org/10.1002/aoc.7315> (2024).

26. Ahankar, H., Taghavi Fardood, S. & Ramazani, A. One-pot three-component synthesis of tetrahydrobenzo[b]pyrans in the presence of $\text{Ni}_{0.5}\text{Cu}_{0.5}\text{Fe}_2\text{O}_4$ magnetic nanoparticles under microwave irradiation in solvent-free conditions. *Iran. J. Catal.* **10**, 195–201 (2020).
27. Chandiran, K. *et al.* Long single crystalline $\alpha\text{-Mn}_2\text{O}_3$ nanorods: Facile synthesis and photocatalytic application. *Mater. Res. Express* **7**, 074001. <https://doi.org/10.1088/2053-1591/ab9fbd> (2020).
28. Gnanam, S. & Rajendran, V. Facile hydrothermal synthesis of alpha manganese sesquioxide ($\alpha\text{-Mn}_2\text{O}_3$) nanodumb-bells: Structural, magnetic, optical and photocatalytic properties. *J. Alloys Compd.* **550**, 463–470. <https://doi.org/10.1016/j.jallcom.2012.10.172> (2013).
29. Moradnia, F., Ramazani, A., Taghavi Fardood, S. & Gouranlou, F. A novel green synthesis and characterization of tetragonal-spinel MgMn_2O_4 nanoparticles by tragacanth gel and studies of its photocatalytic activity for degradation of reactive blue 21 dye under visible light. *Mater. Res. Express* **6**, 075057 (2019).
30. Moradnia, F. *et al.* Magnetic $\text{Mg}_{0.5}\text{Zn}_{0.5}\text{FeMnO}_4$ nanoparticles: Green sol-gel synthesis, characterization, and photocatalytic applications. *J. Clean. Prod.* **288**, 125632 (2021).
31. Moradnia, F., Taghavi Fardood, S., Ramazani, A. & Gupta, V. K. Green synthesis of recyclable MgFeCrO_4 spinel nanoparticles for rapid photodegradation of direct black 122 dye. *J. Photochem. Photobiol. A: Chem.* **392**, 112433 (2020).
32. Kiani, M. T., Ramazani, A. & Taghavi Fardood, S. Green synthesis and characterization of $\text{Ni}_{0.25}\text{Zn}_{0.75}\text{Fe}_2\text{O}_4$ magnetic nanoparticles and study of their photocatalytic activity in the degradation of aniline. *Appl. Organomet. Chem.* **37**, e7053. <https://doi.org/10.1002/aoc.7053> (2023).
33. Chen, S., Liu, F., Xiang, Q., Feng, X. & Qiu, G. Synthesis of Mn_2O_3 microstructures and their energy storage ability studies. *Electrochim. Acta* **106**, 360–371. <https://doi.org/10.1016/j.electacta.2013.06.001> (2013).
34. Sing, K. S. Reporting physisorption data for gas/solid systems with special reference to the determination of surface area and porosity (Provisional). *Pure Appl. Chem.* **54**, 2201–2218 (1982).
35. Lai, Y., Meng, M., Yu, Y., Wang, X. & Ding, T. Photoluminescence and photocatalysis of the flower-like nano-ZnO photocatalysts prepared by a facile hydrothermal method with or without ultrasonic assistance. *Appl. Catal. B* **105**, 335–345. <https://doi.org/10.1016/j.apcatb.2011.04.028> (2011).
36. Uma, B. *et al.* Synthesis of CuO samples by co-precipitation and green mediated combustion routes: Comparison of their structural, optical properties, photocatalytic, antibacterial, haemolytic and cytotoxic activities. *Ceram. Int.* **47**, 10355–10369. <https://doi.org/10.1016/j.ceramint.2020.10.223> (2021).
37. Taghavi Fardood, S., Foroootan, R., Moradnia, F., Afshari, Z. & Ramazani, A. Green synthesis, characterization, and photocatalytic activity of cobalt chromite spinel nanoparticles. *Mater. Res. Express* **7**, 015086. <https://doi.org/10.1088/2053-1591/ab6c8d> (2020).
38. Khataee, A., Soltani, R. D. C., Karimi, A. & Joo, S. W. Sonocatalytic degradation of a textile dye over Gd-doped ZnO nanoparticles synthesized through sonochemical process. *Ultrason. Sonochem.* **23**, 219. <https://doi.org/10.1016/j.ulsonch.2014.08.023> (2015).
39. Taghavi Fardood, S. *et al.* Facile green synthesis, characterization and visible light photocatalytic activity of $\text{MgFe}_2\text{O}_4@ \text{CoCr}_2\text{O}_4$ magnetic nanocomposite. *J. Photochem. Photobiol. A: Chem.* **423**, 113621 (2022).
40. Chakrabarti, S. & Dutta, B. K. Photocatalytic degradation of model textile dyes in wastewater using ZnO as semiconductor catalyst. *J. Hazard. Mater.* **112**, 269 (2004).
41. Taghavi Fardood, S., Golfar, Z. & Ramazani, A. Novel sol–gel synthesis and characterization of superparamagnetic magnesium ferrite nanoparticles using tragacanth gum as a magnetically separable photocatalyst for degradation of reactive blue 21 dye and kinetic study. *J. Mater. Sci. Mater. Electron.* **28**, 17002–17008 (2017).
42. Kansal, S. K., Sood, S., Umar, A. & Mehta, S. K. Photocatalytic degradation of Eriochrome Black T dye using well-crystalline anatase TiO_2 nanoparticles. *J. Alloys Compd.* **581**, 392–397. <https://doi.org/10.1016/j.jallcom.2013.07.069> (2013).
43. Honarmand, M., Golmohammadi, M. & Naeimi, A. Green synthesis of SnO_2 -bentonite nanocomposites for the efficient photo-degradation of methylene blue and eriochrome black-T. *Mater. Chem. Phys.* **241**, 122416 (2020).
44. Sadollahkhani, A., Kazeminezhad, I., Nur, O. & Willander, M. Cation exchange assisted low temperature chemical synthesis of $\text{ZnO}@ \text{Ag}_2\text{S}$ core–shell nanoparticles and their photo-catalytic properties. *Mater. Chem. Phys.* **163**, 485–495 (2015).
45. Zhu, J. & Jiang, Z. Electrochemical photocatalytic degradation of Eriochrome Black T dye using synthesized $\text{TiO}_2@ \text{CNTs}$ nanofibers. *Int. J. Electrochem. Sci.* **16**, 210318. <https://doi.org/10.20964/2021.03.55> (2021).

Author contributions

S.T.F. Supervision, Validation, Project administration, Conceptualization, Investigation, Methodology, Manuscript preparation and revision. F.M. Investigation, Implementation of experiments, Methodology, and Manuscript preparation and revision; F.Y.Z. Implementation of experiments, Methodology; S.H. Implementation of experiments, Methodology, Manuscript preparation; M.A.M. Discussion, writing and review; A.R. Validation, discussion, Writing and review; M.S. Validation, Discussion, Writing and review; K.N. Discussion, Writing and review.

Competing interests

The authors declare no competing interests.

Additional information

Correspondence and requests for materials should be addressed to S.T.F. or M.A.M.

Reprints and permissions information is available at www.nature.com/reprints.

Publisher's note Springer Nature remains neutral with regard to jurisdictional claims in published maps and institutional affiliations.



Open Access This article is licensed under a Creative Commons Attribution 4.0 International License, which permits use, sharing, adaptation, distribution and reproduction in any medium or format, as long as you give appropriate credit to the original author(s) and the source, provide a link to the Creative Commons licence, and indicate if changes were made. The images or other third party material in this article are included in the article's Creative Commons licence, unless indicated otherwise in a credit line to the material. If material is not included in the article's Creative Commons licence and your intended use is not permitted by statutory regulation or exceeds the permitted use, you will need to obtain permission directly from the copyright holder. To view a copy of this licence, visit <http://creativecommons.org/licenses/by/4.0/>.

© The Author(s) 2024